The catalase activity of diiron adenine deaminase

Siddhesh S. Kamat,[1] Gregory P. Holmes-Hampton,[1] Ashima Bagaria,[2] Desigan Kumaran,[2] Shane E. Tichy,[3] Tarun Gheyi,[4] Xiaojing Zheng,[5] Kevin Bain,[4] Chris Groshong,[4] Spencer Emtage,[4] J. Michael Sauder,[4] Stephen K. Burley,[4] Subramanyam Swaminathan,[2] Paul A. Lindahl,[1] and Frank M. Raushel[1]*

[1]Department of Chemistry, Texas A&M University, College Station, Texas 77843-3012
[2]Biology Department, Brookhaven National Laboratory, Upton, New York 11973-5000
[3]Agilent Technologies, 5301 Stevens Creek Boulevard, Santa Clara, California 95051
[4]Lilly Biotechnology Center, 10300 Campus Point Drive, San Diego, California 92121
[5]Case Center for Proteomics, Case Western Reserve University, Cleveland, Ohio 44106

Received 5 August 2011; Revised 28 September 2011; Accepted 29 September 2011
DOI: 10.1002/pro.748
Published online 13 October 2011 proteinscience.org

Abstract: Adenine deaminase (ADE) from the amidohydrolase superfamily (AHS) of enzymes catalyzes the conversion of adenine to hypoxanthine and ammonia. Enzyme isolated from *Escherichia coli* was largely inactive toward the deamination of adenine. Molecular weight determinations by mass spectrometry provided evidence that multiple histidine and methionine residues were oxygenated. When iron was sequestered with a metal chelator and the growth medium supplemented with Mn^{2+} before induction, the post-translational modifications disappeared. Enzyme expressed and purified under these conditions was substantially more active for adenine deamination. Apo-enzyme was prepared and reconstituted with two equivalents of $FeSO_4$. Inductively coupled plasma mass spectrometry and Mössbauer spectroscopy demonstrated that this protein contained two high-spin ferrous ions per monomer of ADE. In addition to the adenine deaminase activity, [Fe^{II}/Fe^{II}]-ADE catalyzed the conversion of H_2O_2 to O_2 and H_2O. The values of k_{cat} and k_{cat}/K_m for the catalase activity are 200 s^{-1} and 2.4 × 10^4 M^{-1} s^{-1}, respectively. [Fe^{II}/Fe^{II}]-ADE underwent more than 100 turnovers with H_2O_2 before the enzyme was inactivated due to oxygenation of histidine residues critical for metal binding. The iron in the inactive enzyme was high-spin ferric with g_{ave} = 4.3 EPR signal and no evidence of anti-ferromagnetic spin-coupling. A model is proposed for the disproportionation of H_2O_2 by [Fe^{II}/Fe^{II}]-ADE that involves the cycling of the binuclear metal center between the di-ferric and di-ferrous oxidation states. Oxygenation of active site residues occurs via release of hydroxyl radicals. These findings represent the first report of redox reaction catalysis by any member of the AHS.

Keywords: adenine deaminase; oxidative damage; amidohydrolase superfamily; catalase activity

---

Abbreviations: ADE, adenine deaminase; ADE_{at}, adenine deaminase from *A. tumefaciens;* ADE_{ca}, adenine deaminase from *C. acetobutylicum*; ADE_{ec}, adenine deaminase from *E. coli*; AHS, amidohydrolase superfamily; HOCl, hypochlorous acid; ICP-MS, inductively coupled plasma mass spectrometry; MS, mass spectrometry; NSLS, National Synchrotron Light Source; PDB, Protein Data Bank; ROS, reactive oxygen species.

Additional Supporting Information may be found in the online version of this article.

Grant sponsor: National Institutes of Health; Grant numbers: GM 71790, GM 74945, GM 46441; Grant sponsor: Robert A. Welch Foundation; Grant number: A-840.

*Correspondence to: Frank M. Raushel, Department of Chemistry, P. O. Box 30012, Texas A&M University, College Station, TX 77843-3012. E-mail: raushel@tamu.edu

Introduction

Adenine deaminase (ADE), a member of the amidohydrolase superfamily (AHS), catalyzes the hydrolytic deamination of adenine to hypoxanthine and ammonia as shown in Scheme 1. One of the apparent roles of this enzyme within bacteria is to recycle purine nucleotides and scavenge ammonia. Other enzymes within the AHS catalyze the deamination of *S*-adenosyl homocysteine, adenosine, guanine, cytosine, 8-oxoguanine, and additional aromatic substrates.[1] The three-dimensional structure of ADE from *Agrobacterium tumefaciens* (ADE_{at}; locus tag: Atu4426) has been determined [Protein Data Bank (PDB) id: 3nqb] and the mechanism of action for the enzyme from *Escherichia coli* K12 (ADE_{ec}; locus tag: b3665) has been elucidated.[2] The ADEs from cog1001 are unique members of the AHS, since they require two divalent cations for maximal catalytic activity while the other deaminases from this superfamily require a single divalent cation in the active site.[1,2] The active site structure of ADE from *A. tumefaciens* is presented in Figure 1.

ADEs from various bacterial sources are highly sensitive to the presence of intracellular iron.[2] Unless precautions are taken to exclude the incorporation of iron into the enzyme during protein expression, the isolated enzyme becomes damaged and catalytic activity is severely compromised. However, the diferrous form of ADE_{ec}, made via reconstitution of apoprotein, is remarkably stable, even in the presence of O_2.[2] In this article, we demonstrate that the extreme lability of ADE in the cell is due to the reaction of H_2O_2 with the diferrous form of the enzyme, and suggest that this reaction may serve as a marker for oxidative stress in certain bacteria. [Fe^{II}/Fe^{II}]-ADE catalyzes the disproportionation of H_2O_2 to water and O_2, and the formation of hydroxyl radical and superoxide from the same substrate. The hydroxyl radicals oxygenate multiple amino acid side chains within the active site, thereby abolishing catalytic activity. This work represents the first report of an enzyme in the AHS able to catalyze an oxidation/reduction reaction. A mechanism for the reaction of hydrogen peroxide with the iron-bound form of ADE is proposed.

Results

Isolation of ADE

The gene for ADE_{ec} was expressed in *E. coli* using standard methods.[2,3] However, the identity of the isolated protein could not be verified by mass spectrometry because multiple levels of post-translational modification made the spectrum impossible to interpret. Mass spectrometric analysis of the trypsin-generated fragments (70% coverage) identified the following residues as oxygenated: His-90, His-92, Met-97, Met-98, Met-186, Met-187, His-235, Met-251, Met-254, His-513, and Met-522 (data not shown). Of these residues, His-90, His-92, and His-235 are metal binding residues, based on amino acid sequence identity and the three-dimensional structure of ADE_{at} (PDB: 3nqb). The kinetic constants for the deamination of adenine by oxygenated ADE_{ec} are 2.0 ± 0.3 s^{-1}, 0.8 ± 0.1 mM, and (2.5 ± 0.2) × 10^3 M^{-1} s^{-1} for k_{cat}, K_m, and k_{cat}/K_m, respectively.

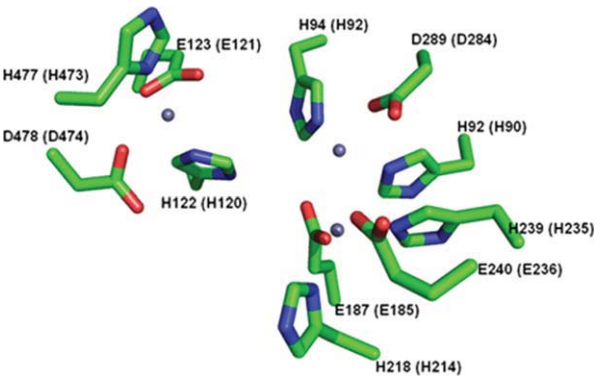

Figure 1. Active site structure of [Mn^{II}/Mn^{II}]-ADE_{at} (PDB id: 3nqb). Residue numbers shown in parentheses are for the equivalent residues from adenine deaminase from *E. coli*. In this structure, there is a third manganese ion bound in the active site that is currently thought to be unimportant for the catalytic activity of adenine deaminase.

The mass spectrum of ADE_{ca} from *C. acetobutylicum* (locus tag: Cac0887) also exhibited multiple species due to oxygenation when expressed in *E. coli* (Supporting Information Fig. S1). Mass spectrometry pinpointed oxygenation sites at His-73, His-75, His-105, His-198, and His-219. Of these residues, His-73, His-75, His-198, and His-219 are metal binding residues by analogy with the structure of ADE_{at}. Tandem mass spectrometry (MS) spectra of two peptides containing residues 94–115 and 194–203 are presented in Supporting Information Figure S2.

Sequestration of iron

It was initially postulated that oxygenation of amino acid residues throughout the protein was initiated by reactions catalyzed by iron bound in the active site of ADE.[2] The addition of 50 μM 2,2'-dipyridyl and 1.0 mM Mn^{2+} to the growth medium was utilized to sequester the iron at the time of induction. ADE_{ec} purified from iron-depleted medium yielded a single species via analysis by mass spectrometry with a molecular weight of 63,741 Da (data not shown; by contrast, the oxygenated enzyme exhibits a broad peak ranging in mass from ~63,600 to ~65,400). Trypsin digestion of this protein gave 91%

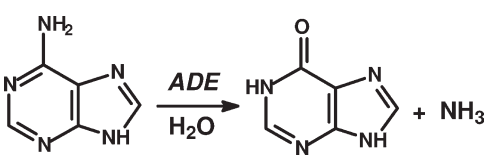

Scheme 1.

Table I. *Kinetic Parameters of ADE Using a Standard and Iron-Free Expression Protocol*

Standard expression protocol					
Locus tag	gi	k_{cat} (s^{-1})	K_m (mM)	k_{cat}/K_m (M^{-1} s^{-1})	Metal content (eq./mol)
b3665	16131535	2.0 ± 0.3	0.8 ± 0.1	(2.5 ± 0.2) × 10^3	0.3 Fe 0.2 Zn
Bh0640	15613203	2.4 ± 0.4	0.20 ± 0.05	(1.2 ± 0.2) × 10^4	0.3 Fe 0.2 Zn
Atu4426	15890557	1.4 ± 0.1	0.20 ± 0.03	(5.0 ± 0.4) × 10^3	0.6 Mn 0.4 Fe
Bsu14520	16078516	1.1 ± 0.4	0.30 ± 0.04	(3.6 ± 0.3) × 10^3	0.2 Fe 0.2 Zn
Cac0887	15894174	0.52 ± 0.02	0.10 ± 0.01	(5.2± 0.3) × 10^3	0.5 Fe 0.1 Zn
Iron-free expression protocol					
Locus tag	gi	k_{cat} (s^{-1})	K_m (mM)	k_{cat}/K_m (M^{-1} s^{-1})	Metal content (eq./mol)
b3665	16131535	200 ± 5	0.40 ± 0.05	(5.0 ± 0.4) × 10^5	2.0 Mn
Bh0640	15613203	120 ± 4	0.30 ± 0.04	(4.0 ± 0.3) × 10^5	1.9 Mn 0.1 Fe
Atu4426	15890557	155 ± 5	0.32 ± 0.03	(4.8 ± 0.3) × 10^5	2.3 Mn
Bsu14520	16078516	140 ± 6	0.40 ± 0.04	(3.5 ± 0.5) × 10^5	1.6 Mn 0.1 Fe
Cac0887	15894174	180 ± 7	0.40 ± 0.05	(4.5 ± 0.4) × 10^5	1.5 Mn 0.1 Fe

sequence coverage and no residues were found to be oxygenated. The total metal content was 2.0 ± 0.1 eq of Mn per protein subunit. Kinetic constants for the deamination of adenine by [Mn^{II}/Mn^{II}]-ADE_{ec}, expressed and isolated by this protocol, are 200 ± 5 s^{-1}, 0.40 ± 0.04 mM, and (5.0 ± 0.4) × 10^5 M^{-1} s^{-1} for k_{cat}, K_m, and k_{cat}/K_m, respectively. The mass spectrum of ADE_{ca}, isolated using the iron-free expression protocol, is presented in Supporting Information Figure S3. Kinetic constants and average metal content for ADE cloned from various bacterial sources and expressed in *E. coli* in the presence and absence of the iron chelator are presented in Table I.

[Mn^{II}/Mn^{II}]-ADE_{ec} was used to prepare apo-ADE_{ec} and this protein was reconstituted with varying amounts of Fe^{2+}, Mn^{2+}, or Zn^{2+}. There was a linear increase in the ADE activity until two equivalents of metal were added.[2,4] Beyond two equivalents of metal per subunit, the deaminase activity remained constant and inductively coupled plasma mass spectrometry (ICP-MS) confirmed the binding of two equivalents of metal per enzyme subunit. This result is only consistent with the cooperative binding of two metal ions in the active site.[4] Previous Mössbauer spectra of the diiron-reconstituted enzyme indicates that both irons are high-spin ferrous, which is denoted as [Fe^{II}/Fe^{II}]-ADE_{ec}.[2]

Inactivation of ADE_{ec} by H_2O_2

A large molar excess of H_2O_2 (250 μM) was added to the metal-reconstituted forms of ADE_{ec} (1.50 μM). Evolution of O_2 was observed when H_2O_2 was added to [Fe^{II}/Fe^{II}]-ADE_{ec}, but not when it was added to either [Mn^{II}/Mn^{II}]-ADE_{ec} or [Zn^{II}/Zn^{II}]-ADE_{ec}. After addition of a large excess of H_2O_2 to [Fe^{II}/Fe^{II}]-ADE_{ec}, the enzyme was unable to catalyze the deamination of adenine, whereas [Mn^{II}/Mn^{II}]-ADE_{ec} and [Zn^{II}/Zn^{II}]-ADE_{ec} had catalytic activities that were unchanged.

Disproportionation of H_2O_2

The initial rate of O_2 evolution catalyzed by [Fe^{II}/Fe^{II}]-ADE_{ec} increased with the concentration of H_2O_2. Kinetic constants for the catalase activity of [Fe^{II}/Fe^{II}]-ADE_{ec} were 200 ± 20 s^{-1}, 9 ± 2 mM, and (2.4 ± 0.5) × 10^4 M^{-1} s^{-1} for k_{cat}, K_m, and k_{cat}/K_m, respectively (based on H_2O_2 consumption). The net increase in the concentration of O_2 produced after addition of an excess of H_2O_2 to [Fe^{II}/Fe^{II}]-ADE_{ec} was proportional to the concentration of added enzyme (Supporting Information Fig. S4). The ratio of O_2 produced, relative to the initial concentration of [Fe^{II}/Fe^{II}]-ADE_{ec}, was 64 ± 3. No O_2 evolution (<1%) was observed for any of the control reactions when 3.0 μM Fe^{2+} was incubated with either EDTA or ascorbate, or by Fe^{2+} itself, when 250 μM H_2O_2 was added. Therefore, the formation of O_2 was due entirely to the catalytic activity of the iron bound to the active site of ADE. Titration of Fe^{2+} to apo-ADE_{ec} (Supporting Information Fig. S5) shows a linear increase in the catalase activity with increasing Fe^{2+} concentration. Maximum catalase activity is observed at two equivalents of Fe^{2+} per monomer of apo-ADE_{ec}.

The time course for O_2 formation after adding 250 μM H_2O_2 to 1.50 μM [Fe^{II}/Fe^{II}]-ADE_{ec} was followed with an oxygen electrode (Fig. 2, open circles). The net change in O_2 concentration was 97 μM (342–245 μM). After O_2 formation ceased, bovine liver catalase was added to determine the concentration of H_2O_2 that remained. The O_2 concentration increased from 342 to 357 μM and thus an

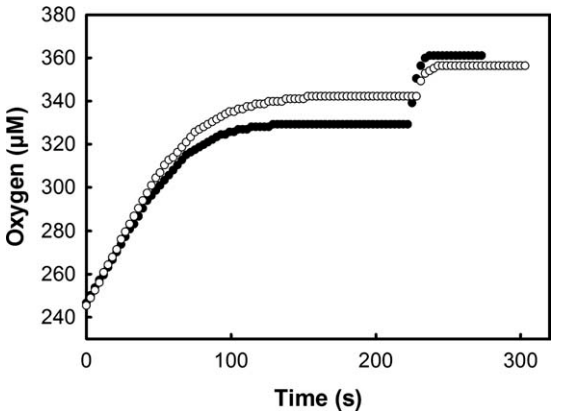

Figure 2. Time course for O_2 formation following the addition of $[Fe^{II}/Fe^{II}]$-ADE_{ec} to an excess of hydrogen peroxide at pH 8.0. Open circles are in the absence of hydroethidine and the closed circles are in the presence of 1.0 mM hydroethidine. After cessation of O_2 evolution, catalase from bovine liver was added to determine the concentration of the unreacted H_2O_2.

additional 15 μM O_2 was produced. Since bovine liver catalase consumes two molecules of H_2O_2 for every O_2 produced, the concentration of H_2O_2 remaining at the time of addition of bovine catalase was 30 μM. Therefore, addition of 1.50 μM $[Fe^{II}/Fe^{II}]$-ADE_{ec} to 250 μM H_2O_2 consumed 220 μM (250–30 μM) hydrogen peroxide and produced 97 μM O_2. Formation of 97 μM O_2 accounts for 194 μM of the hydrogen peroxide consumed. Addition of 3.0 mM 6-chloropurine to a solution containing 1.5 μM $[Fe^{II}/Fe^{II}]$-ADE_{ec} completely inhibited the disproportionation of H_2O_2.

Aliquots were removed after the addition of H_2O_2 to $[Fe^{II}/Fe^{II}]$-ADE_{ec} and then assayed for ADE activity. Deaminase activity decreased, with a first-order rate constant of 0.011 ± 0.001 s^{-1} (data not shown). Mass spectrometry of the tryptic peptides from ADE_{ec} treated with an excess of H_2O_2 demonstrated that the following amino acids were oxygenated: His-90, His-92, Met-97, Met-98, His-176, Met-186, Met-187, Met-251, Met-254, His-513, and Met-522 (data not shown). These are the same residues identified as oxygenated in the protein expressed in *E. coli* without the addition of 2,2'-dipyridyl to sequester the iron before induction.

After cessation of O_2 formation, the H_2O_2-treated ADE_{ec} samples were examined by Mössbauer spectroscopy [Fig. 3(b)]. These samples exhibited a spectral pattern typical of high-spin Fe^{III} ions with rhombic symmetry (E/D ~ 1/3).[5,6] The corresponding electron paramagnetic resonance (EPR) spectrum [Fig. 3(a)] consisted of a g_{ave} ~4.3 signal, typical of such ions. The EPR spin concentration for one sample (190 μM) was comparable with the iron concentration (280 μM). Viewed collectively, these results suggest that the two Fe^{III} ions in the active site are not spin-coupled but are magnetically isolated $S = 5/2$ systems. Typical diferric centers in other enzymes are EPR-silent. Such systems are antiferromagnetically coupled and exhibit quadrupole doublets with δ ~0.5 mm/s and ΔE_Q ~1.1–1.7 mm/s.[7]

Titration of $[Fe^{II}/Fe^{II}]$-ADE with hydrogen peroxide

The amount of O_2 produced when 1–5 molar equivalents of H_2O_2 were added to 20 μM $[Fe^{II}/Fe^{II}]$-ADE_{ec} was determined. After the first equivalent of H_2O_2 was added, 2.2 μM O_2 was formed. The second equivalent of H_2O_2 resulted in formation of 5.9 μM O_2. Sequential addition of three more equivalents of H_2O_2 resulted in the formation of 9.0 μM O_2 with each added equivalent. No O_2 was produced when wild-type $[Fe^{II}/Fe^{II}]$-ADE_{ec} was oxidized by ferricyanide to $[Fe^{III}/Fe^{III}]$-ADE_{ec} before the addition of H_2O_2. Mass spectrometry of ADE_{ec} revealed that the first molar equivalent of H_2O_2 added to untreated $[Fe^{II}/Fe^{II}]$-ADE_{ec} oxygenated either Met-99 or Met-98 while the second molar equivalent oxygenated either His-90 or His-92 (data not shown). The Mössbauer spectra after the addition of one to four equivalents of H_2O_2 to $[Fe^{II}/Fe^{II}]$-ADE_{ec} are presented in Figure 4. In each case, the metal center is found in the diferrous oxidation state.

Detection of superoxide

The formation of superoxide was probed with hydroethidine, a superoxide scavenger.[8] Addition of

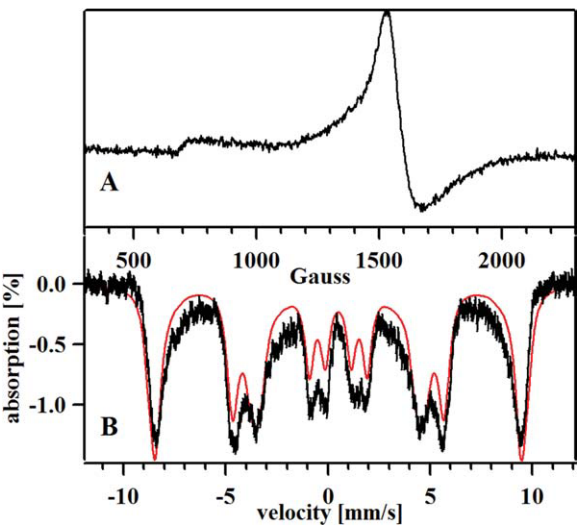

Figure 3. (A) EPR spectrum of 200 μM $[Fe^{III}/Fe^{III}]$-ADE_{ec} formed after the addition of 15 mM H_2O_2 to fresh enzyme. EPR parameters: temperature, 10 K; microwave power, 9.46 GHz, 0.2 mW. (B) Mössbauer spectrum of 200 μM $[Fe^{III}/Fe^{III}]$-ADE_{ec} formed after the addition of 15 mM H_2O_2 to fresh enzyme. The spectrum was collected at 4.5 K, 400 G magnetic field applied parallel to the radiation. Red line represents a simulation of the data with a single species with the following parameters: $D = 0.1$ cm^{-1}; $E/D = 0.33$; $\Delta E_Q = 0.01$ mm/s; $\eta = 3$; $A_x = -250$ kG; $A_y = -240$ kG; $A_z = -230$ kG; $\delta = 0.50$ mm/s; $\Gamma = 0.5$ mm/s.

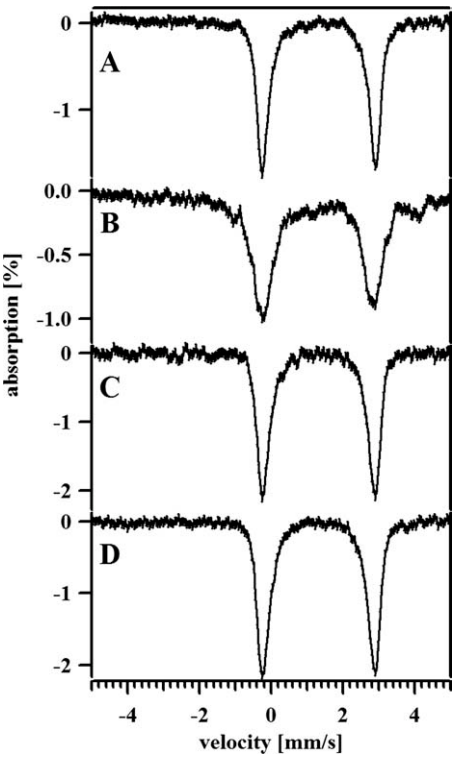

Figure 4. Mössbauer spectra of $[Fe^{II}/Fe^{II}]$-ADE_{ec} with the following number of equivalents of H_2O_2 added to fresh enzyme: (A) 1.0; (B) 2.0; (C) 3.0; and (D) 4.0. Spectra were recorded at 5K with a 700 G magnetic field applied parallel to the radiation. Spectra were fit with a single quadrupole doublet with $\delta = 1.39$ mm/s and $\Delta E_Q = 3.27$ mm/s.

hydroethidine (1.0 mM) to a solution of hydrogen peroxide (256 μM) and $[Fe^{II}/Fe^{II}]$-ADE (1.50 μM) reduced the net production of O_2 from 97 μM (in the absence of hydroethidine) to 81 μM (329–248 μM) (Fig. 2, closed circles). After cessation of O_2 formation, bovine liver catalase was added to the reaction mixture to determine the concentration of the remaining H_2O_2. The O_2 concentration in the solution increased from 329 to 361 μM and thus 64 μM H_2O_2 remained from the initial concentration of 256 μM. The change in absorbance at 470 nm, due to the formation of 2-hydroxyethidium, was 0.20, which corresponds to 17 μM of 2-hydroxyethidium assuming an extinction coefficient of 1.2×10^4 M^{-1} cm^{-1}.[8] This indicates that 17 μM superoxide was formed as 192 μM H_2O_2 was consumed.

Hydroxyl radical formation

Lidocaine is a potent hydroxyl radical scavenger.[9] Addition of a large excess of lidocaine (0.5 M) did not affect the rate of O_2 evolution after 250 μM H_2O_2 was added to 1.5 μM $[Fe^{II}/Fe^{II}]$-ADE_{ec}. When other hydroxyl radical scavengers (thiourea, ethanol, methanol, ethylene glycol, and DMSO) were added at a concentration of 0.50 M, no change was observed in the rates of O_2 evolution and ADE inactivation.

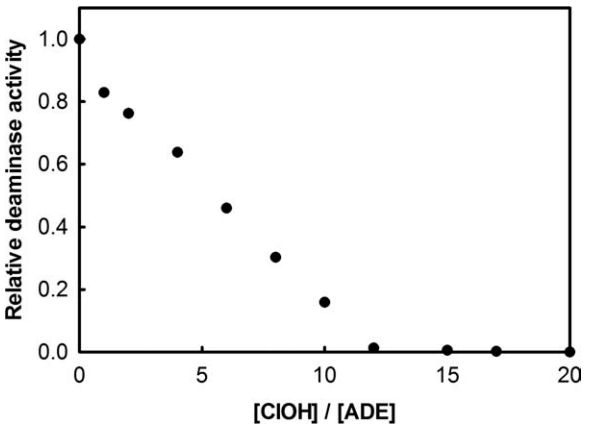

Figure 5. Loss of adenine deaminase activity after addition of HOCl to $[Fe^{II}/Fe^{II}]$-ADE_{ec} (1.0 μM) at 30°C. The deaminase activity was assayed 5 min after addition of HOCl to $[Fe^{II}/Fe^{II}]$-ADE_{ec}.

Hypochlorous acid (HOCl) has been shown to produce hydroxyl radicals in reactions with specific iron complexes.[10] $[Fe^{II}/Fe^{II}]$-ADE_{ec} was titrated with HOCl and ~12 enzyme equivalents of this reagent were needed to inactivate the deaminase activity as shown in Figure 5. Formation of chloride was verified by formation of a precipitate after the addition of silver nitrate. At the end of the reaction of $[Fe^{II}/Fe^{II}]$-ADE_{ec} with HOCl, the iron was found in a high-spin ferric oxidation state (Supporting Information Fig. S6).

Preparation of Mn/Fe hybrids

$[Mn^{II}/Mn^{II}]$-ADE_{ec} is active as a deaminase but not as a catalase. In contrast, $[Fe^{II}/Fe^{II}]$-ADE_{ec} catalyzes both reactions. To determine whether the binuclear metal center of this enzyme must be occupied with two equivalents of iron, or if a manganese/iron hybrid would be sufficient to support catalase

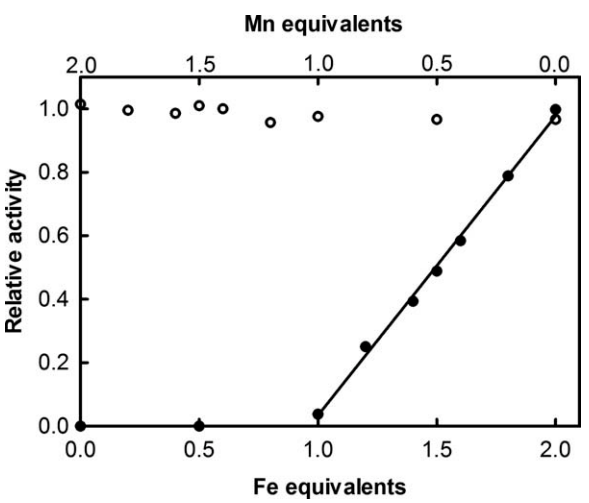

Figure 6. Adenine deaminase (open circles) and catalase activities (closed circles) after apo-ADE_{ec} (1.5 μM) was reconstituted with two enzyme equivalents of total metal (3.0 μM) using various ratios of Mn^{2+} and Fe^{2+}.

Table II. *Catalytic Constants for Deaminase Activity and Metal Content of ADE_{ec} Mutants*

ADE_{ec} mutant	K_m (mM)	k_{cat} (s^{-1})	k_{cat}/K_m (M^{-1} s^{-1})	Metal content (eq. Mn/mol)
Wild type	0.40 ± 0.04	200 ± 5	(5.0 ± 0.4) × 10^5	2.0 ± 0.1
H90N	0.33 ± 0.03	10 ± 0.8	(3.0 ± 0.3) × 10^4	1.8 ± 0.3
S95A	0.47 ± 0.04	98 ± 3	(2.0 ± 0.2) × 10^5	1.8 ± 0.1
D118N	0.36 ± 0.03	170 ± 2	(4.7 ± 0.3) × 10^5	2.1 ± 0.2
H120N	0.49 ± 0.05	0.17 ± 0.02	(3.5 ± 0.2) × 10^2	2.1 ± 0.1
E121Q	0.42 ± 0.04	50 ± 1	(1.2 ± 0.2) × 10^5	1.9 ± 0.2
E236Q	0.40 ± 0.04	0.012 ± 0.002	30 ± 4	1.8 ± 0.1
D284A	0.85 ± 0.07	0.042 ± 0.006	49 ± 5	2.0 ± 0.3
D285A	0.39 ± 0.04	40 ± 2	(1.0 ± 0.2) × 10^5	1.9 ± 0.1
H473N	0.34 ± 0.03	170 ± 2	(5.0 ± 0.3) × 10^5	1.8 ± 0.1
D474N	0.31 ± 0.03	173 ± 4	(5.6 ± 0.2) × 10^5	1.8 ± 0.1

activity, apo-ADE_{ec} (1.5 μM) was reconstituted with two equivalents of metal using a mixture of manganese and iron of different ratios (3.0 μM total metal concentration). ICP-MS verified that the metal content of ADE_{ec} after reconstitution was in accordance with the ratio of metal ions added to apo-ADE_{ec}. ADE activity was independent of the ratio of Mn^{2+} and Fe^{2+} added to the enzyme (Fig. 6). However, no catalase activity was observed until the ratio of iron to manganese exceeded 1.0. When more than one equivalent of iron was added to apo-ADE_{ec}, there was a linear increase in the catalase activity with an increase in the iron content (Fig. 6). These results are consistent with the preferential binding of manganese and/or iron at one of the two metal sites within the binuclear metal center and a requirement for both sites to be occupied by iron for the catalase activity but not the deaminase activity. Apo-ADE_{ec} treated with 1 equivalent each of Mn and Fe exhibited an EPR signal typical of Mn^{II} ions and a Mössbauer spectrum indicative of the high-spin Fe^{II} state (Figs. S7 and S8).

Mutagenesis of ADE

Based on the three-dimensional structure of [Mn^{II}/Mn^{II}]-ADE_{at} (PDB: 3nqb), the metal coordinating residues His-90, Glu-236, and Asp-284 of ADE_{ec} were mutated to asparagine, glutamine, and alanine, respectively, and the mutant proteins were shown to bind two equivalents of metal per protein monomer. Other conserved active site residues, Ser-95, Asp-118, His-120, Glu-121, Asp-285, His-473, and Asp-474 were subsequently chosen as targets for mutagenesis based on their proximity to the binuclear metal center from the structure of ADE_{at}. Of these seven residues, His-120, Glu-121, His-473, and Asp-474 coordinate an adventitiously bound third metal ion found ~6–8Å from the binuclear metal center in ADE_{at} (see Fig. 1). The metal-free forms of these mutants were prepared and reconstituted with Fe^{2+}. ADE activity and metal content of the iron-reconstituted mutants were measured and the results are presented in Table II. The catalase activity of these 10 mutants, except for H473N and D474N, was the same as the wild-type enzyme reconstituted with iron. These two mutants (H473N and D474N) were unable to catalyze the disproportionation of H_2O_2 and were not inactivated by H_2O_2. The diferrous form of the H90N mutant (20 μM) was titrated with 1–5 equivalents of H_2O_2. Unlike wild-type enzyme, this mutant produced ~9 μM O_2 for each equivalent of H_2O_2 added. Mössbauer spectroscopy indicated that ferricyanide treatment of [Fe^{II}/Fe^{II}]-H90N produced the oxidized [Fe^{III}/Fe^{III}]-state. The oxidized H90N mutant catalyzed the disproportionation of H_2O_2.

Measurement of reduction potentials

The reduction potentials for inter-conversion of the diferrous and diferric states of ADE_{ec} were measured with redox-active dyes. In these titrations, it was assumed that both irons in the binuclear metal center are oxidized or reduced in pairs and that the deaminase activity could be used as a direct measure of the relative concentration of [Fe^{II}/Fe^{II}]-ADE_{ec}. Titration of freshly prepared [Fe^{II}/Fe^{II}]-ADE_{ec} (20 μM) with the redox-active oxidant thymol indophenol is presented in Figure 7. A total of 7.9 ± 0.2 equivalents

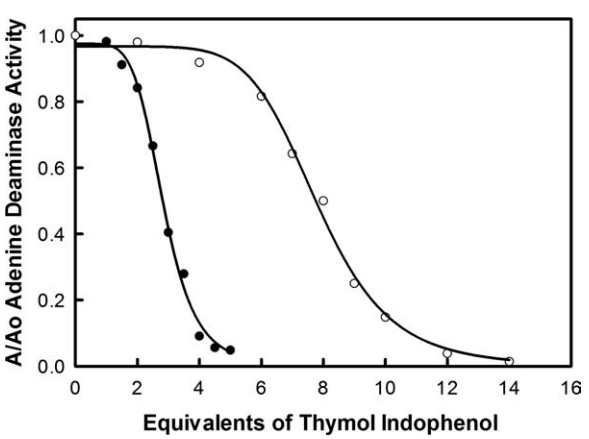

Figure 7. Titration of [Fe^{II}/Fe^{II}]-ADE_{ec} (20 μM) with various amounts of thymol indophenol. The open circles are for enzyme before the addition of hydrogen peroxide. The closed circles are for enzyme after the addition of five equivalents (100 μM) of hydrogen peroxide. Additional details are provided in the text.

of the dye were required to reduce the deaminase activity by 50%. Given the reduction potential of thymol indophenol of +174 mV versus NHE,[11] substitution into Eq. (3) provides an apparent reduction potential of +209 ± 4 mV for interconversion of the diferric and diferrous forms of wild-type ADE. After [Fe^{II}/Fe^{II}]-ADE_{ec} was treated with five equivalents of H_2O_2 it became easier to oxidize the binuclear metal center. Titration of *partially oxygenated* ADE with thymol indophenol is shown in Figure 7. In all, 2.8 ± 0.1 equivalents of thymol indophenol were required to reduce the deaminase activity by 50%. This finding is consistent with a reduction potential of +194 ± 2 mV for the binuclear metal center of partially oxygenated ADE. Addition of thymol indophenol to [Mn^{II}/Mn^{II}]-ADE_{ec} showed no change in catalytic activity indicating that the dye cannot oxidize manganese.

When [Fe^{II}/Fe^{II}]-ADE_{ec} was treated with a large excess of H_2O_2, the binuclear metal center was left in the diferric state, the deaminase activity was lost and not recoverable, even after reduction to the ferrous state using dithionite. Since the ratio of the diferrous and diferric states of the binuclear metal center could not be determined from a direct measurement of the deaminase activity, the distribution of the oxidized and reduced species during the redox titration was determined spectrophotometrically with a dye that is colored in the oxidized state and colorless in the reduced state. The dye crystal violet has a reduction potential of 167 mV.[12] The oxidized form of the dye absorbs at 590 nm with an extinction coefficient of 54,000 M^{-1} cm^{-1}.[12] The reduced form of crystal violet was utilized to reduce the binuclear metal center in fully oxygenated ADE. In this titration, 1.4 ± 0.3 equivalents of the reduced dye were required to reduce 50% of the binuclear metal centers in ADE. Therefore, the reduction potential for the binuclear metal center of [Fe^{III}/Fe^{III}]-ADE^{ox} is +175 ± 4 mV.

The reduction potentials of two mutants, [Fe^{II}/Fe^{II}]-H90N and [Fe^{II}/Fe^{II}]-H473N were measured using thymol indophenol. The manganese-reconstituted enzymes for both of these mutants were used as controls. [Fe^{II}/Fe^{II}]-H90N required 2.6 ± 0.2 enzyme equivalents of thymol indophenol to reduce the ADE activity by 50%. This result translates to a redox potential of +192 ± 4 mV. [Fe^{II}/Fe^{II}]-H473N required 8.0 ± 0.3 equivalents of thymol indophenol to reduce the ADE activity by 50%. The redox potential of [Fe^{II}/Fe^{II}]-H473N from this titration is + 210 ± 6 mV.

pH profiles

The kinetic constants for the catalase activity of [Fe^{II}/Fe^{II}]-ADE_{ec} were obtained as a function of pH (Fig. 8). The profiles for k_{cat} and k_{cat}/K_m exhibited a single ionization for a group that is unprotonated for optimal catalytic activity. The pK_a of this group from the k_{cat} profile is 7.6 ± 0.3, and 7.9 ± 0.2 from the k_{cat}/K_m profile.

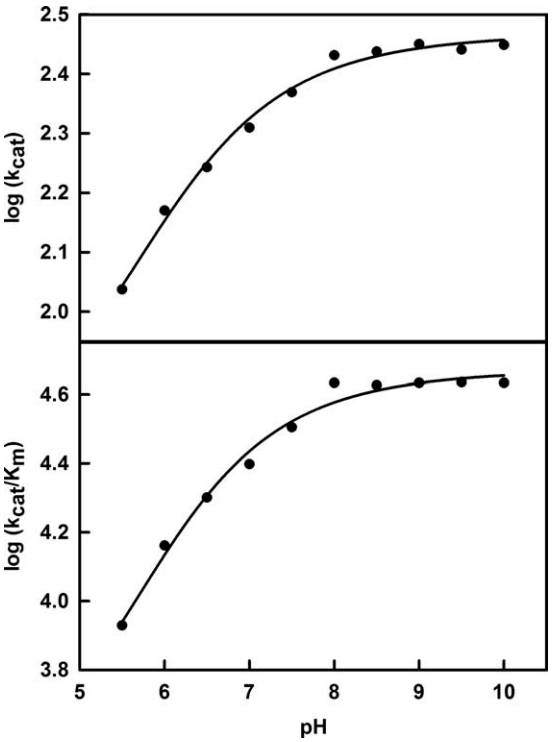

Figure 8. pH rate profiles for the disproportionation of hydrogen peroxide by [Fe/Fe]-ADE_{ec}. The data were fitted to Eq. (2).

Structures of [Fe^{II}/Fe^{II}]-ADE_{at} and [Fe^{II}/Mn^{II}]-ADE_{at}

The three-dimensional structures of the iron/manganese hybrid ([Fe^{II}/Mn^{II}]-ADE_{at}) and the diferrous form ([Fe^{II}/Fe^{II}]-ADE_{at}) of ADE from *A. tumefaciens* were determined to 2.6Å and 2.8Å resolution, respectively. Overall, the structures and active sites of [Fe^{II}/Fe^{II}]-ADE_{at} and [Fe^{II}/Mn^{II}]-ADE_{at} are essentially identical to that of the [Mn/Mn]-ADE_{at} structure determined previously (RMSD is <1Å for all Cα atom pairs). In the [Mn/Mn]-ADE_{at} structure, the active site contains a binuclear manganese center (Mn_α and Mn_β) and a third metal center located 6.6Å from Mn_α.[2] [Fe^{II}/Fe^{II}]-ADE_{at} and [Fe^{II}/Mn^{II}]-ADE_{at} were prepared from apo-ADE_{at} and the metal content for both proteins before crystallization was determined to be 0.95 ± 0.10 Mn, 1.1 ± 0.1 Fe per subunit for the iron/manganese hybrid and 2.1 ± 0.1 Fe per subunit for the diiron ADE by ICP-MS. However, in the crystal structure the active sites of both protein preparations contained three metal ions, similar to the previous structure determined with the di-manganese activated enzyme. In the diferrous form of ADE, Fe_β in the binuclear center and the third metal are five-coordinate, whereas Fe_α is four-coordinate [Fig. 9(a)]. His-92, His-94 (HxH motif), Asp-289, and Glu-187 coordinate Fe_α [Fig. 9(a)]. Glu-

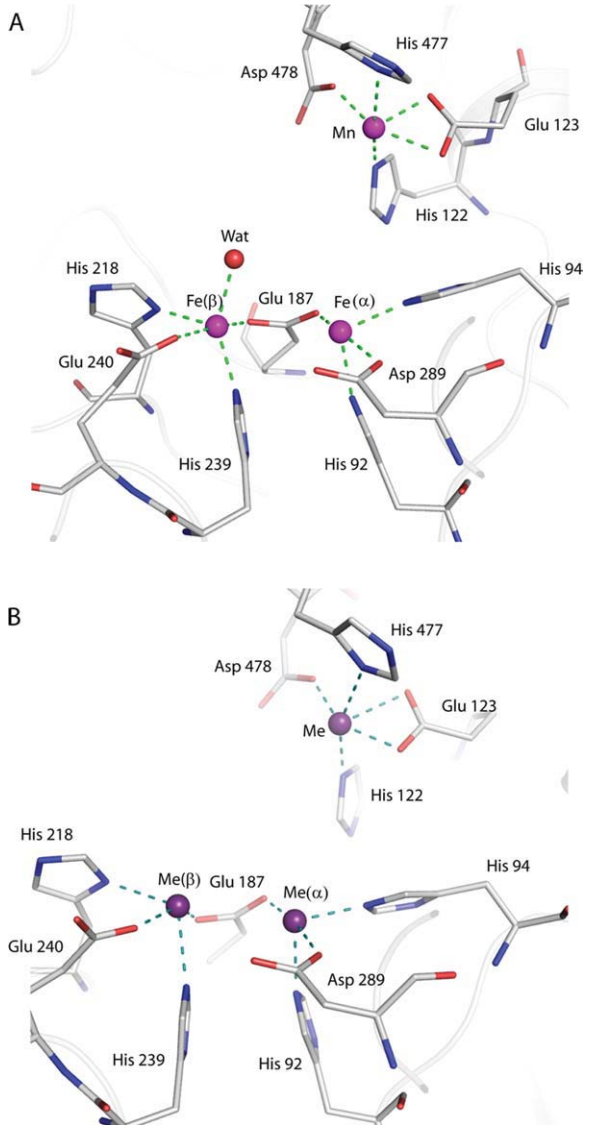

Figure 9. Close up view of the active site of $[Fe^{II}/Fe^{II}]$-ADE_{at} (A) and $[Fe^{II}/Mn^{II}]$-ADE_{at} (B). Grey color ribbon represents the secondary elements at the vicinity of the active site. Active site residues that are coordinating to metals are shown as stick models. Metals and water are shown as spheres.

187, His-218, His-239, Glu-240, and water (W1) coordinate with Fe_β. Glu-187 bridges Fe_α and Fe_β but there is no oxo-bridge as is typical of diiron centers. The Fe_α–Fe_β distance is 4.0Å. Waters that are bridging Mn_α and Mn_β in the [Mn/Mn]-ADE_{at} are not visible in the current structure. The third metal coordinates His-122, Glu-123 (bidendate), His-477, and Asp-478 [Fig. 9(a)]. In the manganese/iron hybrid enzyme, it was not possible to determine the preferential binding locations of the two different metal ions [Fig. 9(b)]. The two metal ions in the binuclear metal center are four-coordinate and the third metal ion is five-coordinate. The coordinating ligands are the same as for $[Fe^{II}/Fe^{II}]$-ADE_{at}, except that there is no water coordination with M_β.

Discussion

Oxidative damage to ADE

When ADEs from cog1001 of the AHS are aerobically expressed in *E. coli*, the isolated enzymes are largely inactive and multiple histidine and methionine residues are damaged by oxygenation. The oxidative damage can be completely eliminated if the iron in the medium is sequestered by an iron-specific chelator before induction of protein expression. Enzymes isolated under these conditions contain two manganese ions in the active site and the turnover numbers for the deamination of adenine are approximately two orders of magnitude greater than for any ADE previously reported in the literature.[2,3] The oxygenation reactions are consistent with generation of a reactive oxygen species (ROS) from the iron-bound form of ADE with a physiological oxidant such as H_2O_2.[13] Apo-ADE can be readily prepared from the undamaged manganese-activated enzyme and reconstituted with two equivalents of manganese, zinc, or iron. The diferrous form of ADE, $[Fe^{II}/Fe^{II}]$-ADE_{ec}, has been utilized here to unravel the mechanism for oxidative damage to this enzyme.

Inactivation with hydrogen peroxide

In the presence of excess H_2O_2, $[Fe^{II}/Fe^{II}]$-ADE_{ec} rapidly loses its ability to deaminate adenine. EPR and Mössbauer spectroscopy of the inactivated enzyme demonstrate that the iron in the active site is in an uncoupled high-spin ferric oxidation state. The metal ions can be reduced back to the di-ferrous state with dithionite but the deaminase activity is not recovered. Therefore, addition of an excess of H_2O_2 to $[Fe^{II}/Fe^{II}]$-ADE_{ec} irreversibly modifies the protein and stabilizes the $[Fe^{III}/Fe^{III}]$ state. Mass spectrometric analysis of the trypsin-treated enzyme confirms that multiple histidine and methionine residues within the protein are oxygenated and that the labeling pattern is identical to enzyme expressed in *E. coli* in the absence of an iron chelator. These results are consistent with generation of a ROS such as hydroxyl radical or superoxide by reaction of H_2O_2 with the binuclear iron center of ADE.

Discovery of catalase activity

Addition of H_2O_2 to $[Fe^{II}/Fe^{II}]$-ADE_{ec} results in the formation of O_2. The catalase-like activity diminishes over the course of a few minutes and is lost in approximately the same time-frame as the deaminase activity. More than 100 turnovers occur before the enzyme is completely inactivated. The promiscuous catalase activity of $[Fe^{II}/Fe^{II}]$-ADE is as fast as the deamination reaction, but significantly slower than other catalases.[14,15] There is no effect by H_2O_2 with either $[Mn^{II}/Mn^{II}]$-ADE or $[Zn^{II}/Zn^{II}]$-ADE and thus the oxidation reactions are specific for the iron-reconstituted enzyme.

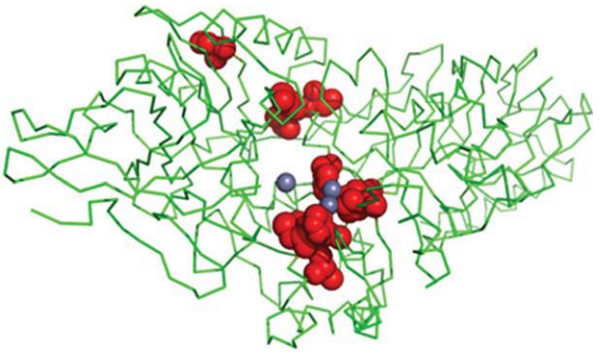

Figure 10. Map of the oxygenation sites following H_2O_2 addition to [Fe^{II}/Fe^{II}]-ADE. The protein backbone is represented in green and the red spheres represent the amino acid side chains that were oxygenated.

The apparent reaction stoichiometry for the catalase-like activity of [Fe^{II}/Fe^{II}]-ADE_{ec} changes as a function of enzyme oxygenation. When one equivalent of H_2O_2 is added to fresh [Fe^{II}/Fe^{II}]-ADE_{ec} that had not been previously exposed to H_2O_2, ~0.11 equivalents of O_2 are produced. After the second equivalent of H_2O_2 is added, ~0.29 equivalents of O_2 are produced. Additional H_2O_2 results in the formation of ~0.45 equivalents of O_2 for every H_2O_2 added. However, the stoichiometry for a physiological catalase is 0.50 equivalents of O_2 for every H_2O_2 utilized.[14,15] These results are, therefore, consistent with leakage of single electron products from the active site, including hydroxyl radical and superoxide.

Formation of superoxide was probed with hydroethidine. When this reagent is added to a reaction mixture containing [Fe^{II}/Fe^{II}]-ADE_{ec} and an excess of hydrogen peroxide, the formation of 2-hydroxyethidium is detected. The amount of 2-hydroxyethidium produced is consistent with ~11 equivalents (17 μM/1.50 μM) of superoxide produced for every enzyme inactivated. During this process, ~54 (81 μM/1.50 μM) equivalents of O_2 are produced and ~128 (192 μM/1.50 μM) equivalents of H_2O_2 are consumed, leaving ~9 equivalents (128-108-11) of H_2O_2 unaccounted. This latter number approximates the number of oxidized histidine and methionine residues sites detected by mass spectrometry that most likely occur from the reaction of hydroxyl radicals with the protein.

It is likely that oxygenation of methionine residues is of minor importance for changes in catalytic activity. However, oxygenation of four histidine residues that coordinate the two irons in the active site can modulate oxidation/reduction reactions via changes in the reduction potential and/or coordination geometry of the binuclear metal center. From the structure of ADE from *A. tumefaciens* (PDB: 3nqb), the oxygenation sites are mapped and shown in Figure 10. These oxygenation sites are predominantly in and around the binuclear metal center and seem to migrate from there to other parts of the protein. This result is consistent with the conclusion that the catalase activity originates at the binuclear metal center and is further supported by the fact that 6-chloropurine, a potent inhibitor of the deaminase reaction, inhibits the catalase activity.

The reduction potential of the binuclear metal center changes with protein oxygenation. For enzyme not previously exposed to H_2O_2, the reduction potential for the inter-conversion of the ferric and ferrous forms of [Fe/Fe-ADE] is +209 mV. When the protein is partially oxygenated, the reduction potential decreases to +194 mV and decreases further to +175 mV when the protein is fully oxygenated and the enzyme is unable to catalyze either the deaminase or catalase reactions. These findings are consistent with the continuous modulation of the catalytic properties of the binuclear iron center as hydroxyl radicals escape and react directly with the metal ligands.

Proposed mechanism of action

How does the binuclear iron center in ADE catalyze the oxidation and reduction of hydrogen peroxide? EPR and Mössbauer spectroscopy demonstrated that the enzyme can cycle between the diferrous and diferric states of oxidation. We have not observed any spectra that are consistent with a ferryl-oxo species (Fe(IV)=O), although this latter species is likely to be too unstable to be detected by the methods employed in this investigation.[14–16] Both metal ions within the binuclear metal center must be iron. A unique Mn/Fe hybrid can be prepared, but it is not known which of the two sites within the binuclear metal center is occupied by iron and which by manganese. This hybrid is completely inactive for reaction with hydrogen peroxide (Fig. 7).

Scheme 2 presents a working model to explain the development and decay of the catalase-like

induction phase

$$[Fe^{II}/Fe^{II}]\text{-ADE} + H_2O_2 + H^+ \rightarrow [Fe^{II}/Fe^{III}]\text{-ADE} + H_2O + {}^{\cdot}OH$$

$$[Fe^{II}/Fe^{III}]\text{-ADE} + {}^{\cdot}OH \rightarrow [Fe^{II}/Fe^{II}]\text{-ADE}^{ox} + H^+$$

sustaining phase

$$[Fe^{II}/Fe^{II}]\text{-ADE}^{ox} + H_2O_2 + 2\,H^+ \rightarrow [Fe^{III}/Fe^{III}]\text{-ADE}^{ox} + 2\,H_2O$$

$$[Fe^{III}/Fe^{III}]\text{-ADE}^{ox} + H_2O_2 \rightarrow [Fe^{II}/Fe^{II}]\text{-ADE}^{ox} + O_2 + 2\,H^+$$

$$[Fe^{III}/Fe^{III}]\text{-ADE}^{ox} + H_2O_2 \rightarrow [Fe^{II}/Fe^{III}]\text{-ADE}^{ox} + HO_2 + H^+$$

$$[Fe^{II}/Fe^{III}]\text{-ADE}^{ox} + H_2O_2 \rightarrow [Fe^{II}/Fe^{II}]\text{-ADE}^{ox} + HO_2 + H^+$$

death phase

$$[Fe^{II}/Fe^{II}]\text{-ADE}^{ox} + H_2O_2 + H^+ \rightarrow [Fe^{II}/Fe^{III}]\text{-ADE}^{ox} + H_2O + {}^{\cdot}OH$$

$$[Fe^{II}/Fe^{III}]\text{-ADE}^{ox} + {}^{\cdot}OH \rightarrow [Fe^{II}/Fe^{II}]\text{-ADE}^{\mathbf{ox\text{-}ox}} + H^+$$

$$[Fe^{II}/Fe^{II}]\text{-ADE}^{\mathbf{ox\text{-}ox}} + H_2O_2 \rightarrow [Fe^{III}/Fe^{III}]\text{-ADE}^{\mathbf{ox\text{-}ox}} + 2\,H_2O$$

Scheme 2.

activity of iron-substituted ADE. We propose that the observed changes in enzyme reactivity are due to changes in the redox properties and structural changes to the diiron center as the protein becomes oxygenated. When H_2O_2 is first added to [Fe^{II}/Fe^{II}]-ADE, the predominant reaction is the formation of water and a hydroxyl radical that is coupled with the transient formation of [Fe^{II}/Fe^{III}]-ADE. The hydroxyl radical subsequently reacts with histidine and methionine residues that are near the active site. The initial odd-electron oxygenated product loses an electron that subsequently reduces the mixed-valent binuclear center back to [Fe^{II}/Fe^{II}]-ADE. This form of the protein is represented as [Fe^{II}/Fe^{II}]-ADE^{ox} in Scheme 2. This induction phase is similar to the reaction of [Fe^{II}/Fe^{II}]-ADE with HOCl. With this substrate, the reaction products are chloride anion and hydroxyl radical, and the protein is initially left as a mixed-valent [Fe^{II}/Fe^{III}]-ADE complex. Since the enzyme can react with approximately 12 molecules of HOCl before the enzyme is inactivated, the active site must therefore cycle between the [Fe^{II}/Fe^{II}]-ADE and [Fe^{II}/Fe^{III}]-ADE oxidation states. The initial odd-electron products from the reaction of methionine and histidine residues must lose an electron that reduces [Fe^{II}/Fe^{III}] back to [Fe^{II}/Fe^{II}]. However, HOCl differs from H_2O_2 since it cannot be oxidized.

During the induction phase of the reaction of ADE with H_2O_2, the direct metal ligands to the binuclear metal center become oxygenated (Scheme 2). This effect lowers the reduction potential of the binuclear metal center from +209 V to +194 V that apparently enables the enzyme to cycle between the [Fe^{II}/Fe^{II}] and [Fe^{III}/Fe^{III}] states in a sustaining phase. Mutation of the four histidine residues that coordinate the two active site irons suggests that the oxidation of His-90 is the key modification for the transition from the induction phase to the sustaining phase. During this stage, the stoichiometry of the catalase reaction is not perfect and there is continual leakage of the ROS, hydroxyl radical, and superoxide, which continue to oxygenate the protein. Eventually, the enzyme enters the final death phase after multiple residues within the active site become oxygenated. This form of the enzyme is represented as [Fe^{III}/Fe^{III}]-$ADE^{ox–ox}$ in Scheme 2. At this point, the reduction potential of the metal center is lowered to +174 V and the diferric form of ADE can no longer be reduced to the diferrous state by hydrogen peroxide. Modulation of the catalytic properties of the binuclear iron center may occur with changes in the reduction potential but changes in catalytic activity may also be the result of conformational changes in the metal center itself.

When an excess of H_2O_2 is added to ADE in the presence of a superoxide scavenger, ~128 enzyme equivalents of hydrogen peroxide are consumed and ~54 equivalents of O_2 are produced. The other products are hydroxyl radicals and ~11 equivalents of superoxide. Since inclusion of hydroxyl radical scavengers had no effect on the kinetics of O_2 formation, it appears that the hydroxyl radicals are fully trapped by the protein and do not escape to the bulk solvent. Based on the number of residues found to be oxidized after ADE is no longer active, approximately 10–12 enzyme equivalents of hydroxyl radicals are produced for every enzyme molecule inactivated. This value is very similar to the number of HOCl molecules that are required to fully inactivate ADE.

During the sustaining phase, the predominant reaction is the conversion of hydrogen peroxide to O_2 and water. However, there is significant formation of hydroxyl radical and superoxide that must occur via single electron transfers. Oxidation and reduction of H_2O_2 during the sustaining phase may occur by two single electron transfers to form superoxide and hydroxyl radical intermediates or by a coupled two-electron transfer to form O_2 and water directly. The mechanism proposed for the disproportionation of hydrogen peroxide by [Fe/Fe]-ADE is similar to that of dimanganese catalase found in some organisms, where the enzyme uses Mn^{II}/Mn^{II} and Mn^{III}/Mn^{III} as the metal center to catalyze the conversion of hydrogen peroxide to oxygen and water via a coupled two electron transfer process.[17,18] Interestingly, [Mn^{II}/Mn^{II}]-ADE exhibits no catalase activity, presumably because this state may lack sufficient reducing power to reduce H_2O_2 to water.

We further propose that hydrogen peroxide binds to the binuclear metal center and that single and/or coupled two electron transfers occur to and from these two metal ions. However, in all ADE crystal structures obtained thus far there are three metal ions in the active site even though the crystallizations were initiated with protein with only two metals per subunit. It is not clear how the third metal ion was incorporated into the protein during crystallization. ICP-MS analysis demonstrated that there were only two metal ions bound per subunit before crystallization. There are four protein residues that coordinate the third metal ion in ADE_{ec}: His-120, Glu-121, His-473, and Asp-474. His-473 and Asp-474 form an invariant and fully conserved HD dyad in all ADEs in cog1001 and are absolutely critical for the catalase activity but have no role in the deaminase activity. The pH rate profiles for the catalase activity indicate that a single group must be unprotonated for catalytic activity with a pK_a of 7.6–7.9. This pK_a value is consistent with His-473 serving in proton transfer reactions in the oxidation and reduction of hydrogen peroxide. Computational docking to the three-dimensional structure of ADE_{tu} suggests that His-120 is required to hydrogen bond to N3 of adenine.[2]

Comparison with other catalases

Catalase activity is supported by various types of metal sites, including hemes,[14,15] binuclear

manganese centers,[17,18] and a few binuclear iron centers.[5,6] The latter are found in monooxygenase enzymes and model compounds.[5,6,19] Perhaps the best studied of these is toluene/*o*-xylene monooxygenase from *Pseudomonas* sp. OX1.[6] For this enzyme, the two irons are anti-ferromagnetically coupled and the diferric form is stable in air. This is typical for diiron centers that have no catalase activity. Structurally characterized diiron centers in their oxidized states have an oxo bridging group with Fe–Fe distances of ca. 3.5Å. In contrast, the irons in ADE are further separated, lack a bridging oxo group and are not anti-ferromagnetically coupled. The diferrous form is also stable in air. These properties impact the redox potentials that modulate catalase activity. Perhaps the longer Fe–Fe distance in ADE discourages oxo bridge formation which destabilizes the [Fe^{III}/Fe^{III}] state, such that this state oxidizes H_2O_2 to O_2, leaving the more stable [Fe^{II}/Fe^{II}] state.

Potential physiological significance

The physiological significance of the inherent catalase activity of ADE substituted with iron is unclear. However, it is known that in certain bacteria the deamination of adenine can function as a key step in the purine salvage pathway for formation of guanine nucleotides.[20] Therefore, under conditions of oxidative stress inactivation of ADE would block formation of guanine nucleotides via the purine salvage pathway, which in turn might slow cell growth under conditions of oxidative stress. There are known bacterial transcription factors that use metal-catalyzed oxidation of histidine (via H_2O_2) as a redox sensor for controlling oxidative stress levels in cells. For example, PerR uses iron in the ferrous oxidation state to oxidize a histidine residue critical for DNA binding, thereby regulating oxidative stress levels within cells.[21,22] Another example is the iron enzyme ribulose-5-phosphate 3-epimerase, which is irreversibly inactivated with H_2O_2, presumably from Fenton chemistry catalyzed by Fe^{2+} in the active site. This enzyme can be protected by incorporation of manganese in the active site.[23]

It is apparent that there is insufficient catalase in the cell when *E. coli* is grown aerobically to reduce the hydrogen peroxide concentration to a level that does not inactivate ADE. The catalytic domain of ADE comprises the N-terminal half of the protein and there is a rather large C-terminal domain of approximately 300 amino acids that has no obvious function. The N-terminal half of the protein is required for coordination of the binuclear metal center and encompasses all of the residues necessary for the deaminase activity. The C-terminal domain has the highly conserved HD dyad. Mutation of these residues results in the total loss of the catalase activity but has absolutely no effect on the deaminase activity. These two residues are postulated to function in proton transfers during conversion of H_2O_2 to H_2O and O_2.

The promiscuous catalase activity is not limited to ADE from *E. coli*. We have also interrogated ADEs from *B. subtilis (*Bsu14520), *A. tumefaciens (*Atu4426), *B. halodurans* (Bh0640), and *C. acetobutylicum* (Cac0887). All of these enzymes catalyze the deamination of adenine and all catalyze the disproportionation of hydrogen peroxide when iron is bound to the active site. Members of the AHS catalyze hydrolytic, hydration, decarboxylation,[24] and isomerization reactions.[25,26] This work revealed the first instance of a redox-type reaction from this superfamily of enzymes. It is, therefore, interesting to consider that other enzymes of unknown function within this superfamily will catalyze similar reactions.

Materials and Methods

Materials

All chemicals were purchased from Sigma-Aldrich unless otherwise stated. *Escherichia coli* BL21(DE3) and XL1-blue competent cells were obtained from Stratagene. The expression vector pET30a(+), *Pfx Platinum* DNA polymerase and *Pfu Turbo* DNA polymerase were purchased from Invitrogen.

ADE from E. coli *and* A. tumefaciens

Cloning of ADE from *E. coli* (ADE_{ec}) and *A. tumefaciens* (Atu4426; gi|15890557) was performed as described.[2] Mutations to these proteins were constructed using the QuikChange PCR protocol according the manufacturer's instructions. Enzymes were expressed and purified using an iron-free expression protocol.[2] The deamination of adenine was followed spectrophotometrically at 340 nm.[2]

ADE from other sources

Clones for ADE from *Bacillus halodurans* (Bh0640; gi|15613203), *Bacillus subtilis* (Bsu14520; gi|16078516) and *Clostridium acetobutylium* (Cac0887; gi|15894174) were expressed in an HY SeMet medium (Orion Enterprises, Northbrook, IL). Overnight cultures were prepared from glycerol stocks that were derived from fresh transformants in LB medium for 18 h at 37°C. A 5–10% inoculum was achieved by adding 50–100 mL of an overnight culture to 1 L of SeMet medium containing 30 μg/mL kanamycin, 30 μg/mL chloramphenicol, and 10 mL of 50% glycerol in a 2 L baffled shake flask. Cultures were grown at 37°C to an $OD_{600} = 0.8$. SeMet buffer (90 mg/L) was introduced and the culture was allowed to stand for 20 min at 22°C, after which 0.4 mM IPTG was added to induce the culture and grown for another 18 h at 225 rpm agitation. Cells were harvested using standard centrifugation for 10 min at 5500*g* and frozen at −80°C until ready for

purification. Cell pellets produced from 1 L *E. coli* cell cultures expressing the C-terminal His-tagged proteins were suspended in 250 mL of lysis buffer (50 mM Tris–HCl pH 7.7, 250 mM NaCl, and six tablets of Roche Complete, EDTA-free protease inhibitor cocktail). The suspension was lysed by sonication and insoluble debris was removed by centrifugation for 30 min (39,800*g*). The supernatant was collected and incubated with 10 mL of a 50% slurry of Qiagen Ni-NTA Agarose, which was pre-equilibrated with wash buffer (20 mM Tris–HCl pH 8.0, 500 mM NaCl, 10% glycerol, and 25 mM imidazole) for 30 min with gentle stirring. The sample was then poured onto a drip column and washed with 50 mL of wash buffer to remove the unbound proteins. Protein was eluted using 25 mL of the elution buffer (wash buffer with 500 mM imidazole). The eluted fraction was further purified by gel filtration chromatography on a GE Healthcare HiLoad 16/60 Superdex 200 prep grade column that was pre-equilibrated with gel filtration buffer (10 mM HEPES, pH 7.5, 150 mM NaCl, 10% glycerol, and 5 mM DTT). The best fractions were combined and concentrated by centrifugation in an Amicon Ultra-15 10,000 Da MWCO centrifugal filter unit.

Preparation of [Fe^{II}/Fe^{II}]-ADE

Apo-ADE was reconstituted by the anaerobic addition of two equivalents of Fe^{2+}.[2] Samples were subsequently passed through a PD-10 column to remove unbound metal.[2] The stoichiometry of the reconstituted metal center was determined by anaerobic titration of apo-ADE (10 μM) with Fe^{2+}. The metal content was determined by ICP-MS.

Measurement of catalase activity

Formation of O_2 was determined with a YSI 5300A biological oxygen monitor at 30°C. Standard assay conditions were 20 mM HEPES, pH 7.5, variable amounts of H_2O_2 and enzyme in a final volume of 3.0 mL. The H_2O_2 concentration was calibrated with an oxygen electrode and bovine liver catalase. The H_2O_2 concentration was also measured spectrophotometrically at 240 nm using a molar extinction coefficient of 43.6 M^{-1} cm^{-1}.[27] For control experiments, 250 μM H_2O_2 was added to a buffered solution containing 3.0 μM Fe^{2+} and 1.0 mM EDTA, or 3.0 μM Fe^{2+}, 1.0 mM EDTA, and 1.0 mM ascorbate.

Redox titrations

The reduction potential of [Fe^{II}/Fe^{II}]-ADE_{ec} was determined with the redox dye, thymol indophenol (TCI America). [Fe^{II}/Fe^{II}]-ADE_{ec} (20 μM) was incubated with 2–14 equivalents of thymol indophenol in 20 mM HEPES, pH 7.5, at room temperature for 4 h. Similar experiments were conducted with [Fe^{II}/Fe^{II}]-ADE_{ec} treated previously with five equivalents of H_2O_2. Determination of the reduction potential of fully oxygenated [Fe^{II}/Fe^{II}]-ADE_{ec} was conducted with protein that had been treated previously with 3.0 mM H_2O_2. The excess H_2O_2 was removed by passage through a PD-10 column. Reduced crystal violet was used to reduce the oxidized binuclear metal center back to the di-ferrous state in 20 mM HEPES, pH 7.5. Concentrations of the oxidized and reduced forms of the dye were determined at 590 nm after 6 h of incubation.

Mass spectrometry

ADE_{ec} (5 μg) was loaded onto a 10% SDS-PAGE gel. The Coomasie Blue-stained protein band was excised from the gel, cut into pieces, and digested with trypsin (Promega). The excised gel bands were washed with 25 mM ammonium bicarbonate, pH 8.0, dehydrated with 50 μL of a 2:1 mixture of acetonitrile/50 mM ammonium bicarbonate for 5 min and then dried in a vacuum centrifuge. Gel pieces were further rehydrated for 40 min in an ice bath with 20 μM trypsin (Promega) in 25 mM ammonium bicarbonate buffer to a final volume of 12 μL. Following rehydration, samples were digested for 4 h at 37°C.

Digested gel slices (1–2 μL) were analyzed by tandem MS (Agilent 6520 quadrupole time-of-flight instrument with chip cube electrospray ionization). Samples were injected using a protein chip (160-nL trap, 75 × 150 mm, 5 μm, C-18 SB-Zorbax, 300Å) at a flow rate 300 nL/min. Data acquisition was performed using MassHunter (version B.02.00) in a 2-GHz extended dynamic range at a rate of three scans per second followed by data-dependent tandem mass spectrometric fragment scans of the four most intense ions. Precursor ion exclusion was set to 6 s after two consecutive tandem mass spectrometric scans. Acquired tandem mass spectrometric spectra were analyzed against a trypsin-specific enzyme search within Spectrum Mill (Agilent Technologies) with the defined protein sequence.

For intact mass analysis of ADE from *B. halodurans*, *A. tumefaciens*, *B. subtilis*, and *C. actobutylium*, matrix-assisted laser desorption/ionization (MALDI, Voyager-DE) and liquid chromatography electrospray ionization mass spectrometry (LC-ESI-MS, Agilent 1100, API150EX) were used to assess the purity and measure accurate masses of proteins. ESI-MS data were acquired in positive ion mode and spectra were deconvoluted using BioAnalyst 1.4 software to obtain 200 ppm mass accuracy. For site-specific modification studies, MS/MS analysis was performed using a linear trap quadropole Fourier transform (LTQ-FT) mass spectrometer (Thermo Finnigan) coupled with an Ultimate 3000 high performance liquid chromatography (Dionex). Following reduction and *S*-alkylation, protein in 50 mM Tris-HCl (pH 8.0) was digested overnight by trypsin, Asp-N (Roche Diagnostic), and chymotrypsin (Roche Diagnostic), respectively. Aliquots of the samples (1 pmol) were analyzed online using nanoflow high performance liquid chromatography-

Table III. *X-ray Data Collection and Refinement Statistics*

Name/code	$[Fe^{II}/Fe^{II}]$-ADE_{at}	$[Fe^{II}/Mn^{II}]$-ADE_{at}
Unit cell dimensions	$a = 61.7$Å, $b = 131.8$Å, $c = 69.6$Å; $\beta = 97.0°$	$a = 61.5$Å, $b = 131.2$Å, $c = 69.3$Å; $\beta = 97.0°$
Space group	$P2_1$	$P2_1$
Resolution limit (Å)	50–2.63 (2.68–2.63)	50.0–2.8 (2.85–2.8)
Unique reflections	32849	26874
Completeness, %	99.6 (93.9)	99.7 (97.0)
Rmerge[a],	0.1 (0.78)	0.17(0.60)
Refinement statistics		
No. of protein atoms	8614	8672
No. of metal atoms	6	6
No. of solvent atoms	54	83
Rcryst	0.185	0.174
Rfree	0.287	0.30
Root mean square deviations		
Bond distance (Å)	0.04	0.02
Bond angles (°)	1.9	1.96
Ramachandran plot statistics (%)		
Residues in allowed regions	87.2	86.0
Residues in additionally allowed regions	11.4	12.8
Average B-factors (Å^2) for chains A and B		
Main chain (A, B)	30.8, 35.7	40.3, 47.4
Sidechain (A, B)	32.1, 37.1	41.6, 48.4
Solvent (A, B)	25.6	31.5
Metal atoms	54.3	48.8
PDB ID	3T81	3T8L

[a] $R_{merge} = \sum |I_i - \langle I \rangle| / \sum |I_i|$ where I_i is the intensity of the ith measurement, and $\langle I \rangle$ the mean intensity for that reflection. Values for the highest resolution shell are given within parentheses.

nanoelectrospray ionization. Data were acquired in positive ion mode. Peptides were sequenced by tandem mass spectrometry and identified by Mascot (Matrix Science, Version 2.1) search. Significant hits were manually inspected.

EPR and Mössbauer spectroscopy

Samples for EPR and Mössbauer spectroscopy were made and data were collected as described previously.[2]

Titration with HOCl

$[Fe^{II}/Fe^{II}]$-ADE_{ec} (1.0 μM) was treated with HOCl ranging from 0–20 μM for 5 min at 30°C, pH 7.5. At the end of the reaction, the ADE activity was determined as described.[2] In addition, HOCl (200 μM) was added to 16 μM $[Fe^{II}/Fe^{II}]$-ADE_{ec} and the absorbance spectrum was measured. The same experiments were performed with $[Mn^{II}/Mn^{II}]$-ADE_{ec} as a control. The concentration of HOCl was determined at 292 nm ($\varepsilon = 3241\ M^{-1}\ cm^{-1}$).[28]

Detection of superoxide

Formation of superoxide was measured using the dye hydroethidine (Invitrogen). Concentration of hydroethidine was determined at 345 nm ($\varepsilon = 9.75 \times 10^3\ M^{-1}\ cm^{-1}$).[8] Hydroethidine reacts with superoxide to form 2-hydroxyethidium which was monitored at 470 nm ($\varepsilon = 1.2 \times 10^4\ M^{-1}\ cm^{-1}$).[8] $[Fe^{II}/Fe^{II}]$-ADE_{ec} (1.50 μM) was mixed with 1.0 mM hydroethidine in a final volume of 3.0 mL in a YSI 5300A biological oxygen monitor system at 30°C. Hydrogen peroxide (250 μM) was added and the evolution of O_2 was measured as a function of time. After O_2 production ceased, 1.0 mL from this reaction mixture was removed and the absorbance was measured at 470 nm.

pH-rate profiles

The pH dependence of k_{cat} and k_{cat}/K_m for the catalase activity was determined for $[Fe^{II}/Fe^{II}]$-ADE_{ec} over the pH range of 5.5–10.0. The buffers used for this study were 20 mM MES (pH 5.5–6.5), 20 mM HEPES (7.0–8.0), and 20 mM CHES (pH 8.5–10.0). The pH values of the solutions were measured before and after the completion of the assays.

6-Chloropurine inhibition of catalase activity

A solution of $[Fe^{II}/Fe^{II}]$-ADE_{ec} (1.5 μM) was incubated with 3.0 mM 6-chloropurine for 1 h in 50 mM HEPES buffer, pH 7.5 and then assayed for ADE and catalase activity as described previously.[2]

Data analysis

Initial velocity kinetic data were fit to Eq. (1) using SigmaPlot 9.0 where v is the initial velocity, [A] is the substrate concentration, E_t is the total enzyme concentration, k_{cat} is the turnover number, and K_m is the Michaelis constant. For pH-rate profiles, Eq. (2) was used to fit the half-bell shaped pH profiles to determine values of pK_a for the ionization of residues at low pH. In Eq. (2), the value of c is the

maximum value for either k_{cat} or k_{cat}/K_m, depending on the fit, and H is the proton concentration. In Eq. (3), E is the reduction potential of the metal center, E^o is the reduction potential of the dye, R is the universal gas constant, T is the temperature, n is the number of electrons transferred during the redox reaction, and F is the Faraday constant. A_{ox} is the concentration of the species involved in the oxidation reaction of the enzyme and A_{red} is the concentration of the species involved in the reduction reaction of the enzyme.

$$v/E_t = k_{cat}[A]/(K_m + [A]) \quad (1)$$

$$\log y = \log[c/(1 + H/K_a)] \quad (2)$$

$$E = E^o - (RT \ln[A_{red}]/[A_{ox}])/nF \quad (3)$$

Structure determination of Atu4426

The iron/manganese hybrid ($[Fe^{II}/Mn^{II}]$-ADE_{at}) and the diferrous form ($[Fe^{II}/Fe^{II}]$-ADE_{at}) of ADE were crystallized via sitting drop vapor diffusion at room temperature using conditions similar to those reported for [Mn/Mn]-ADE_{at}.[2] Before data collection, crystals were transferred into mother liquor containing 20% glycerol and then flash cooled in liquid nitrogen. Data were collected at 100 K on beam line X29 at the National Synchrotron Light Source (NSLS). Diffraction data were processed with HKL-2000.[29] Data collection and refinement statistics are summarized in Table III. Structures were determined by rigid-body refinement of native model lacking metal followed by restrained refinement in REFMAC.[30] Metals were identified from the difference Fourier map and subsequent model building was carried out in COOT.[31] Geometry of the final refined models was evaluated using PROCHECK.[32] The refined final atomic coordinates and structure factor amplitudes were evaluated and deposited in the PDB. The PDB entries are 3T81 and 3T8L for $[Fe^{II}/Fe^{II}]$-ADE_{at} and $[Fe^{II}/Mn^{II}]$-ADE_{at}, respectively.

Acknowledgments

The authors thank Ryan Blasé from the Laboratory of Biological Mass Spectrometry, Texas A&M University for performing some of the preliminary mass spectrometry experiments. They also thank the NYSGXRC protein production team. The plasmids should be available at DNASU (http://dnasu.asu.edu/), with external clone IDs: 9206a1BCt6p1 (Atu4426), 9207a2BSt3p1 (Bh0640), 9207b1BCt4p1 (Bsu14520), and 9211b1BCt18p1 (Cac0887).

References

1. Seibert CM, Raushel FM (2005) Structural and catalytic diversity within the amidohydrolase superfamily. Biochemistry 44: 6383–6391.
2. Kamat SS, Bagaria A, Desigan K, Holmes-Hampton GP, Fan H, Sali A, Sauder JM, Burley SK, Lindahl PA, Swaminathan S, Raushel FM (2011) Catalytic mechanism and three dimensional structure of adenine deaminase. Biochemistry 50: 1917–1927.
3. Petersen C, Moller LB, Hansen PV (2002) The cryptic adenine deaminase gene from *Escherichia coli*. J Biol Chem 277: 31373–31380.
4. Shim H, Raushel FM (2000) Self-assembly of the binuclear metal center of phosphotriesterase. Biochemistry 39: 7357–7364.
5. Dewitt JG, Bentsen JG, Rozenweig AC, Hedman B, Green J, Pilkinton S, Papaefthymiou GC, Dalton H, Hodgson KO, Lippard SJ (1991) X-ray absorption, Mössbauer and EPR studies on the diiron center in the hydroxylase component of methane monooxygenase: evidence for a hydroxide bridge. J Am Chem Soc 115: 9219–9235.
6. Murray LJ, Naik SG, Ortillo DO, Serres RG, Lee JK, Huynh BH, Lippard SJ (2007) Characterization of the arene-oxidizing intermediate in ToMOH as a diiron(III) species. J Am Chem Soc 129: 14500–14510.
7. Fox BG, Surerus KK, Münck E, Lipscomb JD (1988) Evidence for a mu-oxo binuclear iron cluster in the hydroxylase component of methane monooxygenase: Mössbauer and EPR studies. J Biol Chem 263: 10553–10556.
8. Zielonka J, Vivar JV, Kalyanaraman B (2008) Detection of 2-hydroxyethidium in cellular systems: a unique marker product of superoxide and hydroethidine. Nat Prot 3: 8–21.
9. Das KC, Misra HP (1992) Lidocaine: a hydroxyl radical scavenger and singlet oxygen quencher. Mol Cell Biochem 115: 179–185.
10. Dukan S, Toutati D (1996) Hypochlorous Acid stress in *Escherichia coli:* resistance, DNA damage and comparison with hydrogen peroxide stress. J Bacteriol 178: 6145–6150.
11. Jacob HE (1970) Methods in microbiology. In: Redox Potential. New York: Academic Press, pp 94–95.
12. Sukumaran VS, Ramalingam A (2006) Spectral characteristics and nonlinear studies of crystal violet dye. Spectrochem Acta 63: 673–676.
13. Kurtz DM (2006) Avoiding high-valent iron intermediates: superoxide reductase and ruberythrin. J Inorg Biochem 100: 679–693.
14. Bertini I, Gray HB, Stiefel EI, Valentine JS (2006) Biological inorganic chemistry. In: Peroxidase and catalases, Chapter: XI. 3. Sausalito, CA, Poulos, TL: University Science Books, pp 343–354.
15. Messerchmidt et al. (2001) Handbook of metalloproteins 1. In: Heme catalases. New York: John Wiley & Sons, pp 486–502.
16. Imlay JA (2008) Cellular defenses against superoxide and hydrogen peroxide. Annu Rev Biochem 77: 755–776.
17. Waldo GS, Penner-Hahn JE (1995) Mechanism of manganese catalase peroxide disproportionation: determination of manganese oxidation states during turnover. Biochemistry 34: 1507–1512.
18. Barynin VV, Whittaker MM, Antoyuk SV, Lamzin VS, Harrison PM, Artymiuk PJ, Whittaker JW (2001) Crystal structure of manganese catalase from *Lactobacillus plantarum*. Structure 9: 725–738.
19. Friedle S, Kodanko JJ, Morys AJ, Hayashi T, Loccoz PM, Lippard SJ (2009) Modeling the syn disposition of nitrogen donors in non-heme diiron enzymes. Synthesis, characterization, and hydrogen peroxide reactivity of diiron(III) complexes with syn N-donor ligand H_2BPG_2DEV. J Am Chem Soc 131: 14508–14520.
20. Nygaard P, Duckert P, Saxild HH (1996) Role of adenine deaminase in purine salvage and nitrogen

metabolism and characterization of *ade g*ene in *Bacillus subtilis*. J Bacteriol 178: 846–853.
21. Lee J, Helmann JD (2006) The perR transcription factor senses H_2O_2 by metal catalysed histidine oxidation. Nature 340: 363–367.
22. Moye WSR (2006) Redox sensing and histidine oxidation: no longer perfect strangers. Nat Chem Biol 5: 234–235.
23. Sobota JM, Imlay JA (2011) Iron enzyme ribulose-5-phosphate 3-epimerase in *Escherichia coli* is rapidy damaged by hydrogen peroxide but can be protected by manganese. PNAS 108: 5402–5407.
24. Liu A, Zhang H (2006) Transition metal-catalyzed non-oxidative decarboxylation reactions. Biochemistry 45: 10407–10411.
25. Nguyen TT, Brown S, Federov AA, Federov EV, Babbitt PC, Almo SC, Raushel FM (2008) At the periphery of the amidohydrolase superfamily: Bh0493 from *Bacillus halodurans* catalyzes the isomerization of D-galacturonate to D-tagaturonate. Biochemistry 47: 1194–1206.
26. Nguyen TT, Federov AA, Williams L, Federov EV, Li Y, Xu C, Almo SC, Raushel FM (2009) The mechanism of the reaction catalyzed by uronate isomerase illustrates how an isomerase may have evolved from a hydrolase within the amidohydrolase superfamily. Biochemistry 48: 8879–8890.
27. Noble RW, Gibson QH (1970) The reaction of ferrous horseradish peroxidase with hydrogen peroxide. J Biol Chem 245: 2409–2413.
28. Hartmann T, Hartmann PP, Wetteland C, Lu N (2003) Spectroscopic determination of hypochlorous acid, in chloride brine solutions, featuring 5 MeV proton beam line experiments. Rad Phys Chem 66: 335–341.
29. Otwinowski Z, Minor W (1997) Processing of X-ray diffraction data collected in oscillation mode. Methods Enzymol 276: 307–326.
30. Murshudov GN, Vagin AA, Dodson EJ (1997).Refinement of macromolecular structures by the maximum-likelihood method. Acta Crystallogr.D53: 240–255.
31. Emsley P, Cowtan K (2004) Coot: model-building tools for molecular graphics. Acta Crystallogr.D60: 2126–2132.
32. Laskowski RA, MacArthur MW, Moss DS, Thornton JM (1993) PROCHECK: a program to check the stereochemical quality of protein structures. J Appl Cryst 26: 283–291.